

Automatic Detection of Magnetic δ in Sunspot Groups

Sreejith Padinhatteeri^{1,2} · Paul
A. Higgins^{1,3} · D. Shaun Bloomfield¹ · Peter
T. Gallagher¹

© Springer

Abstract

Large and magnetically complex sunspot groups are known to be associated with flares. To date, the Mount Wilson scheme has been used to classify sunspot groups based on their morphological and magnetic properties. The most flare prolific class, the δ sunspot-group, is characterised by opposite polarity umbrae within a common penumbra, separated by less than 2° . In this article, we present a new system, called the Solar Monitor Active Region Tracker - Delta Finder (SMART-DF), that can be used to automatically detect and classify magnetic δ s in near-realtime. Using continuum images and magnetograms from the *Helioseismic and Magnetic Imager (HMI)* onboard NASA's *Solar Dynamics Observatory (SDO)*, we first estimate distances between opposite polarity umbrae. Opposite polarity pairs having distances of less than 2° are then identified, and if these pairs are found to share a common penumbra, they are identified as a magnetic δ configuration. The algorithm was compared to manual δ detections reported by the Space Weather Prediction Center (SWPC), operated by the National Oceanic and Atmospheric Administration (NOAA). SMART-DF detected 21 out of 23 active regions (ARs) that were marked as δ spots by NOAA during 2011–2012 (within $\pm 60^\circ$ longitude). SMART-DF in addition detected five ARs which were not announced as δ spots by NOAA. The near-realtime operation of SMART-DF resulted in many δ s being identified in advance of NOAA's daily notification. SMART-DF will be integrated with SolarMonitor* and the near-realtime information will be available to the public.

¹ School of Physics, Trinity College Dublin, Dublin 2, Ireland email: sreejith.p@gmail.com

² Manipal Centre for Natural Sciences, Manipal University, Manipal, Karnataka, India - 576104.

³ Lockheed Martin Advanced Technology Center, Dept/A021S, B/252, 3251 Hanover Street, Palo Alto, CA 94304, USA.

*www.solarmonitor.org

1. Introduction

Solar flares are among the most energetic events in the solar system (energy up to $\sim 10^{25}$ J; Emslie *et al.*, 2012; Moore *et al.*, 2001; Aschwanden and Freeland, 2012) influencing a panorama of physical systems, from the solar surface through the heliosphere and onwards into geospace. Flares, along with coronal mass ejections (CMEs), are a major contributor to space weather – the interaction of magnetic fields and particles accelerated on or near the Sun with the Earth’s magnetosphere and upper atmosphere (Gopalswamy *et al.*, 2005; Messerotti *et al.*, 2009; Hapgood and Thomson, 2010). Although significant progress has been made in understanding the fundamental physics of solar flares and coronal mass ejections, accurate forecasting of these enigmatic events remains elusive (Gallagher, Moon, and Wang, 2002; Cui *et al.*, 2006; Leka and Barnes, 2007; Yuan *et al.*, 2010).

Flares occur in the volume of atmospheric plasma above sunspot groups. Sunspot groups are formed by the convective action of sub-surface fluid motions pushing magnetic flux tubes through the Sun’s surface, the photosphere. Turbulent photospheric and subphotospheric motions jostle these flux tubes and, when the conditions are right, the sunspots produce a flare (*e.g.*, Conlon *et al.*, 2008). Currently the exact conditions that lead to flaring are not known. The analysis of sunspot groups and their properties has allowed the most accurate flare prediction to date (Barnes and Leka, 2008; Bloomfield *et al.*, 2012; Ahmed *et al.*, 2013).

Studying large volumes of data to identify sunspot groups and their various properties is generally done using feature-characterisation and tracking algorithms. The automatic detection of sunspots and their constituent structures has been investigated using photospheric intensity images (Zharkov *et al.*, 2004; Curto, Blanca, and Martínez, 2008) and magnetograms (McAteer *et al.*, 2005; LaBonte, Georgoulis, and Rust, 2007; Lefebvre and Rozelot, 2004). Various feature tracking algorithms were developed as part of the Heliophysics Events Knowledgebase (HEK; Martens *et al.*, 2012). Verbeeck *et al.* (2013) provide a review of the robustness of four major algorithms used to automatically detect and characterise active regions (ARs) and sunspot groups. The algorithms that they discuss are: the Solar Monitor Active Region Tracker (SMART; Higgins *et al.*, 2011), an automated AR detection and characterisation algorithm that uses magnetograms to detect magnetic features; the Automated Solar Activity Prediction code (ASAP; Colak and Qahwaji, 2008, 2009), a set of algorithms that uses intensity images and machine learning to detect and predict flares; the Sunspot Tracking and Recognition Algorithm (STARA; Watson *et al.*, 2009); and the Spatial Possibilistic Clustering Algorithm (SPOCA; Barra *et al.*, 2009). A comparative study of flare prediction between SMART-ASAP (a combination of the feature detection of SMART and the machine learning of ASAP) and ASAP was performed in Ahmed *et al.* (2013), which found SMART-ASAP to be the more accurate.

Sunspot groups have traditionally been classified using the McIntosh (McIntosh, 1990) and Mount Wilson (Hale *et al.*, 1919) classification schemes. The

McIntosh scheme classifies the complexity of sunspot groups from their white-light structure, whereas the Mount Wilson scheme uses magnetograms to classify the spatial distribution of magnetic polarities.

The original Mount Wilson classification scheme consisted of unipolar (α), bipolar (β) and mixed polarity (γ) designations, before being extended into the current Mount Wilson scheme through the addition of the δ designation – opposite polarity umbrae being enclosed by a common penumbra (Künzel, 1960, 1965). A statistical investigation of the connection between δ spots and major solar flares was published by Sammis, Tang, and Zirin (2000), finding that the vast majority of X-class flares occur from sunspot groups that display a δ configuration at some time. However, Mount Wilson classifications are only issued every 24 hours by the National Oceanic and Atmospheric Administration (NOAA) Space Weather Prediction Center (SWPC), so it remains unclear how long it takes to produce a major flare after a δ spot forms. Automated detection of δ spot formation from high-cadence data is necessary to answer this, with real-time implementation being beneficial for flare forecasting. Here, a new software module named SMART-Delta Finder (SMART-DF) is developed as an extension of the SMART algorithm to automatically detect and characterise δ spots using simultaneous intensity and magnetogram data.

In this paper, the SMART-DF algorithm is explained in Section 2. The SMART-DF code is tested on several individual cases, with Section 3 presenting the observation and data analysis. Section 4 includes the results and Section 5 presents the conclusions and discussion of this work.

2. SMART-DF Algorithm

SMART-DF is a software package developed using Interactive Data Language (IDL) and SolarSoft (Freeland and Handy, 1998). The definition of the δ classification as per Künzel (1965) is simply, a sunspot group with a “common penumbra enclosing opposite polarity umbrae”. Mt. Wilson Observatory uses a more specific definition for δ spots as “umbrae separated by less than 2° within one penumbra have opposite polarity”¹. The only addition in this definition, compared to Künzel (1965), is the specific value for the maximum distance between two opposite polarity umbrae. SMART-DF is developed based on this definition, and hence the distance threshold between the two opposite polarity umbrae is kept as 2° . This algorithm implements the following two conditions for δ detection. First, the region should have two opposite polarity umbrae with centroids separated by less than 2° heliographic distance. Second, these two umbrae should be surrounded by a common penumbra. These two conditions must be satisfied to classify a sunspot group as a δ spot. In SMART-DF the candidates that satisfy the first condition are named δ candidates, while those that satisfy both conditions are labelled as δ spots.

A simultaneously observed photospheric intensity image and line-of-sight (LOS) magnetogram are the necessary input to the code. The code also uses some

¹www.swpc.noaa.gov/sites/default/files/images/u2/Glossary.pdf

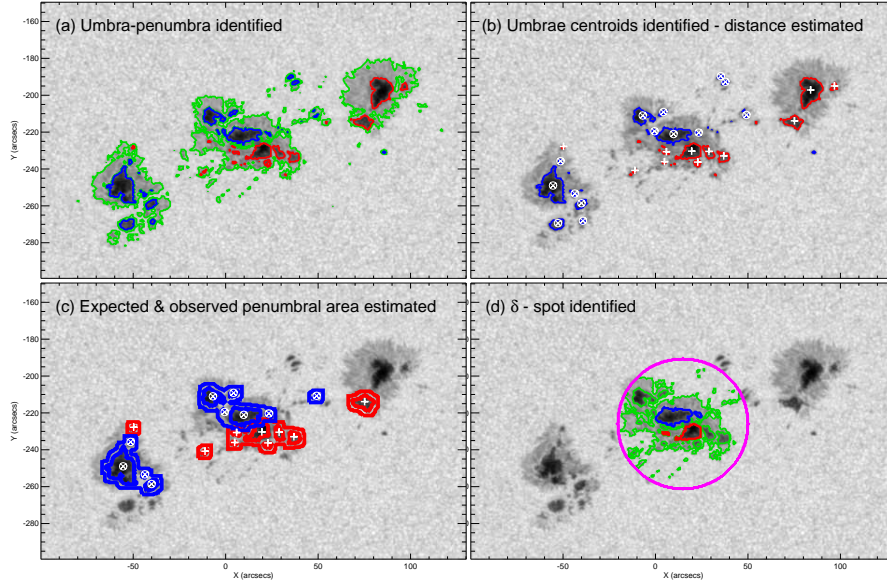


Figure 1. Summary of the SMART-DF algorithm. (a) Umbra-penumbra boundaries are identified using continuum intensities and LOS magnetic field values. Blue (Red) contours mark the negative (positive) umbral border and green contours mark the penumbral boundary. (b) Each umbra is labeled based on area and the centroids are identified and marked. A plus-symbol is used to denote positive and an encircled cross is used to denote negative polarities. Also the distance between each positive-negative pair is estimated. (c) The boundary of expected penumbral regions around those positive (negative) umbrae which pass condition 1 (opposite polarity umbrae within 2°) are marked with a red (blue) contour. (d) If all conditions in the algorithm are satisfied, the identified δ spot is marked with a magenta circle. See Section 2 for a detailed explanation of the SMART-DF algorithm.

parameters which must be provided as input. These include choosing a particular field of view (FOV), instead of full disc, to detect δ spots. When a δ spot is found, SMART-DF will mark the location on an image, along with an output structure providing details of magnetic and geometric properties of the identified features. The values of some input parameters are critical, since they decide the success of detection. The parameters and their optimised values used in this study are listed in Table 1, and the reason for choosing these values for each parameter are explained in Section 3. Figure 1 shows the major steps of the SMART-DF algorithm, which are described in the sections below.

2.1. Umbra-Penumbra Identification

Regions of umbrae and penumbrae are identified using simultaneously observed continuum and magnetogram images. First, the intensity images are corrected for limb-darkening using the Allen (1976) model. For each intensity image, a simultaneous magnetogram is also obtained and cosine-correction is applied to the magnetogram (McAteer *et al.*, 2005). A histogram of continuum intensity for a region with a mature sunspot generally shows a triple-peaked distribution

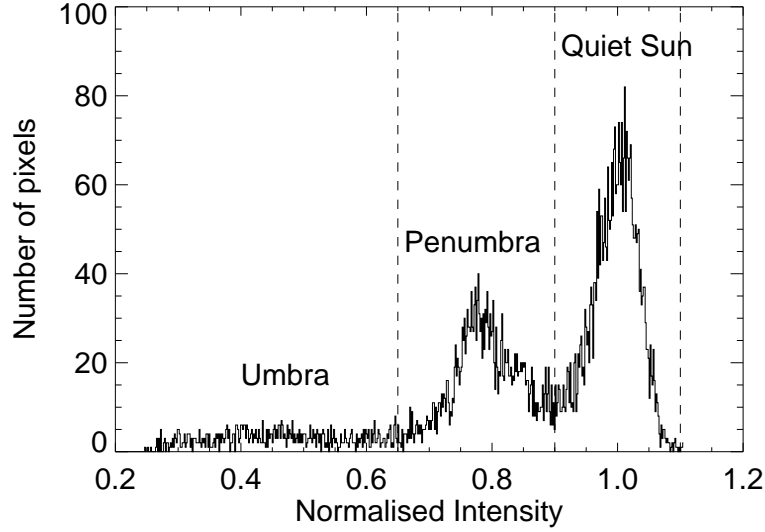


Figure 2. A histogram of the intensity distribution of a mature sunspot that is normalised to the quiet-Sun intensity. The peak at 1.0 corresponds to quiet-Sun pixels, and the other two peaks correspond to penumbrae and umbrae, as indicated in the figure.

as shown in Figure 2. The Mean quiet-Sun intensity is defined as I_{QS} , and intensities less than $0.65 I_{QS}$ correspond to umbral pixels. Similarly, the peak at $\approx 0.77 I_{QS}$ corresponds to the penumbral intensity (Leka and Skumanich, 1998). In this study, all pixels with intensity less than $0.65 I_{QS}$ and with a line-of-sight magnetic-field intensity, $|B_{LOS}| \geq 500$ G are defined as umbral pixels. Similarly, pixels within the intensity range of $0.65 - 0.9 I_{QS}$ are defined as penumbral pixels and above $0.9 I_{QS}$ are defined as quiet Sun. These values are used globally for all images. Also, since our results are not dependent on flux within the umbral area, the errors in the intensity levels used are not important. The above selection procedure is verified manually by plotting contours around the umbra and penumbra. An example can be seen in the top-right image of Figure 1.

2.2. Distance Estimation

To avoid detecting very small pores and inter-granular lanes, only umbrae above a certain minimum cut-off area (A_{min}) are used to detect δ spots. The value used for A_{min} in this study is given in Table 1. Each umbra with an area larger than A_{min} in the FOV is labeled based on its size and polarity. Hence, the largest positive-polarity umbra will be labeled U_1^+ , the next largest as $U_2^+, U_3^+, \dots, U_n^+$ and similarly, $U_1^-, U_2^-, \dots, U_m^-$ for the negative polarity. The distance between each possible pairing of opposite polarity umbrae is calculated. The distance is measured from the center of the umbra, taken as the B_{LOS} weighted centroid. Those pairs of umbrae with a distance of less than 2° in heliographic coordinates are marked as first-level δ candidates, which satisfy the first condition of the

definition at the beginning of this section. Note that each candidate is a pair of positive and negative polarity umbrae, and only these candidates are considered for further analysis.

2.3. Presence of Common Penumbra around Spots

Penumbrae form around the umbrae, with or without azimuthal symmetry. A region around an umbral border with a certain width (the penumbral expected length, P_{el}) is selected and marked as the expected penumbral region ($P_{expected}$). Actual penumbral filaments can be bigger or smaller in size than P_{el} in different cases. Hence, $P_{expected}$ is simply the area around umbrae where we expect to find penumbrae. Based on observed intensity levels, each pixel in this region is marked as either penumbral or non-penumbral. The area of such observed penumbra ($P_{observed}$) inside $P_{expected}$ is calculated. This is done for both the pair of umbrae in each δ candidate. Ideally, if penumbrae are formed with azimuthal symmetry and fill the $P_{expected}$ region, then the ratio $P_{frac} = P_{expected}/P_{observed}$ should be equal to unity. This is not always the case. In most of the cases the penumbra formation is not azimuthally symmetric and in some cases the penumbral size can be less than the width of the $P_{expected}$ region, given by the parameter P_{el} . Hence, expecting such a ratio to be equal to unity is not always practical. The ratio also depends on the value of P_{el} that we choose as input. In this study we have used different values of this ratio to qualify for second-level δ candidates, as explained in Section 4.

The third level checks whether the penumbra around the pair of umbrae are connected. This is done by determining whether $P_{observed}$ around each umbra in the pair is connected (sharing some common area, P_{share}). The pairs of opposite polarity spots that pass the three checks are marked as δ spots. This algorithm becomes unreliable when the active region approaches the limb, due to projection effects of both foreshortening and apparent (*i.e.*, false) LOS magnetic-field polarity inversions. In this paper, we test SMART-DF only for ARs within $\pm 60^\circ$ longitude.

3. Observations and Data Analysis

SMART-DF was tested using data from the *Helioseismic and Magnetic Imager* (HMI; Scherrer *et al.*, 2012). The HMI instrument was developed by the Stanford Solar Group and is a part of NASA's *Solar Dynamic Observatory* (SDO). HMI can be used to obtain continuum intensity images as well as LOS magnetic-field strength of the full solar-disc at high temporal cadence (every 45 seconds). HMI also obtains magnetic-field vector information using polarimetry, but this is not used in this study. The primary input to SMART-DF is a pair of simultaneous continuum intensity images and magnetograms. All the ARs that appear on the solar-disc during 2011 and 2012, with in $\pm 60^\circ$ longitude were analysed to test the reliability of SMART-DF. A pair of intensity images and LOS magnetograms were obtained with 12 hour cadence, *i.e.*, at 00:00 UT and 12:00 UT every day from the archived HMI data. SMART (Higgins *et al.*, 2011) is used to automatically identify ARs and define regions of interest (ROIs) on the solar-disc. All

Table 1. The parameters used by SMART-DF and their optimised values used for this algorithm testing study.

Parameter	Value Used	Details
A_{\min}	1.5 Mm ²	Minimum/cut-off umbral area
P_{el}	3.5 Mm	Expected length of penumbra/rudimentary penumbra
P_{frac}	75%	Ratio of actual penumbra with expected penumbral area
P_{share}	750 km ²	Common shared area between penumbrae of two spots

ARs located within $\pm 60^\circ$ of longitude have been checked for δ configurations using SMART-DF as explained in Section 2. To calculate distances and areas on the solar-disc, firstly helioprojective coordinates are converted to heliographic coordinates using the world coordinate-system (WCS; Greisen and Calabretta, 2002) programs (Thompson, 2006) available in the standard solar data analysis software (SolarSoft SSIDL) and then spherical-trigonometry cosine-law is used (Smart, 1965).

SWPC, operated by NOAA, releases a Solar Region Summary (SRS) text file every day at 00:30 UT. SRS files contain the Hale classification of each AR on disc. NOAA classifies each active region by visually analysing the previous day data. Each day SRS between 1 January 2011 and 31 December 2012 were obtained from the SWPC database and a list of ARs that formed δ configurations was created. Detections of δ spots from SMART-DF were compared with this list and a comparison test was performed using two methods.

The first method tests whether all ARs detected by NOAA as having a δ configuration on a particular day were also detected by SMART-DF. For this, those days on which a new AR appeared on the solar-disc were noted down (based on NOAA numbers in the SRS files). Each AR that formed a δ configuration according to the SRS files during 2011 and 2012 were listed and the date of its first detection as a δ was noted. SRS is based on observations of the Sun the previous day to the ‘release date’. Hence, SMART-DF was used to check for δ configurations in the data of that day (the previous day of the SRS release date that has a δ spot). In this test, SMART-DF is limited to find less than or an equal number of δ spots compared to SRS. The results have been compared and are presented in Section 4 of this paper.

The second method tests the relative detection rates of NOAA/SWPC and SMART-DF. On each day, the number of δ configurations identified by NOAA are counted and plotted as a histogram distribution. Full-disc images (simultaneous continuum and magnetogram) are obtained with a 12-hour cadence, meaning twice per day for each day in 2011 and 2012. SMART-DF was used to look for δ configurations and a similar histogram was created and over-plotted for comparison. SMART-DF can detect less than, equal to or more instances of δ configurations NOAA/SWPC detections.

There are four important input parameters needed to obtain reliable results from SMART-DF, as explained in the previous section (Section 2). They are:

- i) A_{\min} , the minimum umbral area to be counted as an umbra;

- ii) P_{el} , the expected length of a penumbra (or rudimentary penumbra, as it is called in the case of a forming penumbra);
- iii) P_{frac} , the fraction of penumbral area observed with respect to the expected penumbral area.
- iv) P_{share} , the common area shared by the penumbrae of two opposite polarity spots.

The optimisation of these four parameters is critical for successful δ spot detection. The optimised values used for this study are given in Table 1. The optimisation was performed by varying these parameters to find the combinations with the maximum successful detection rate of NOAA detected regions. Users are free to change these values in the code to suit their needs or if they find any anomalous AR going undetected (*e.g.*, see the discussion on NOAA AR 12192 in Section 5). The minimum umbral area required to qualify as an umbra is fixed at 1.5 Mm^2 , which is greater than the typical size-scale of granulation (known to be $\sim 1 \text{ Mm}$; Nordlund, Stein, and Asplund, 2009). The expected length of the penumbra (or rudimentary penumbra) is fixed at 3.5 Mm , the typical size of a forming penumbra (Solanki, 2003). Technically the value of P_{el} could be as large as the minimum distance that is needed to pass condition 1 of a δ spot (*i.e.*, 2° in heliographic coordinate system). However, intergranular lanes and other intensity regions seen in complex active regions can be wrongly marked as penumbra when P_{el} is too large. Hence, it is important to choose an optimal value that matches with typical penumbral length-scales. The third parameter is the fraction of actual penumbral area with respect to expected penumbral area. Ideally this has to be equal to unity (*i.e.*, 100%). However, the actual penumbral length can be different from case to case, and in many cases penumbrae will not be formed completely around both umbrae. Hence if we fix this value to 100%, even if there is a small region without penumbra, the algorithm will fail to count them as a δ candidate. This fraction can be significantly different from case to case, so SMART-DF was tested with different values of P_{frac} on a known δ region. This resulted in an optimal value of 75% for P_{frac} which was used in the rest of this study. This value also depends on the value of P_{el} chosen. The fourth parameter, P_{share} , is fixed at 750 km^2 ($2 \text{ pixels} \times 2 \text{ pixels}$ in the observed data). This is the common area shared between two penumbrae, so that they appear as one common penumbra.

4. Results

The SMART-DF algorithm was tested on multiple ARs. One example can be seen in the bottom-right image in Figure 1. Three other examples of δ spot detection are shown in Figure 3. In each row, the left side shows an HMI photospheric intensity image and the right side shows an HMI LOS magnetogram. The positive (north) and negative (south) polarity umbral areas are marked with red and blue contours, respectively. Green contours mark penumbral areas. A circle is drawn to highlight the region of interest centred at the δ forming region.

In the upper row in Figure 3, two main spots with opposite polarity are observed, with the leading spot having negative polarity and the following spot

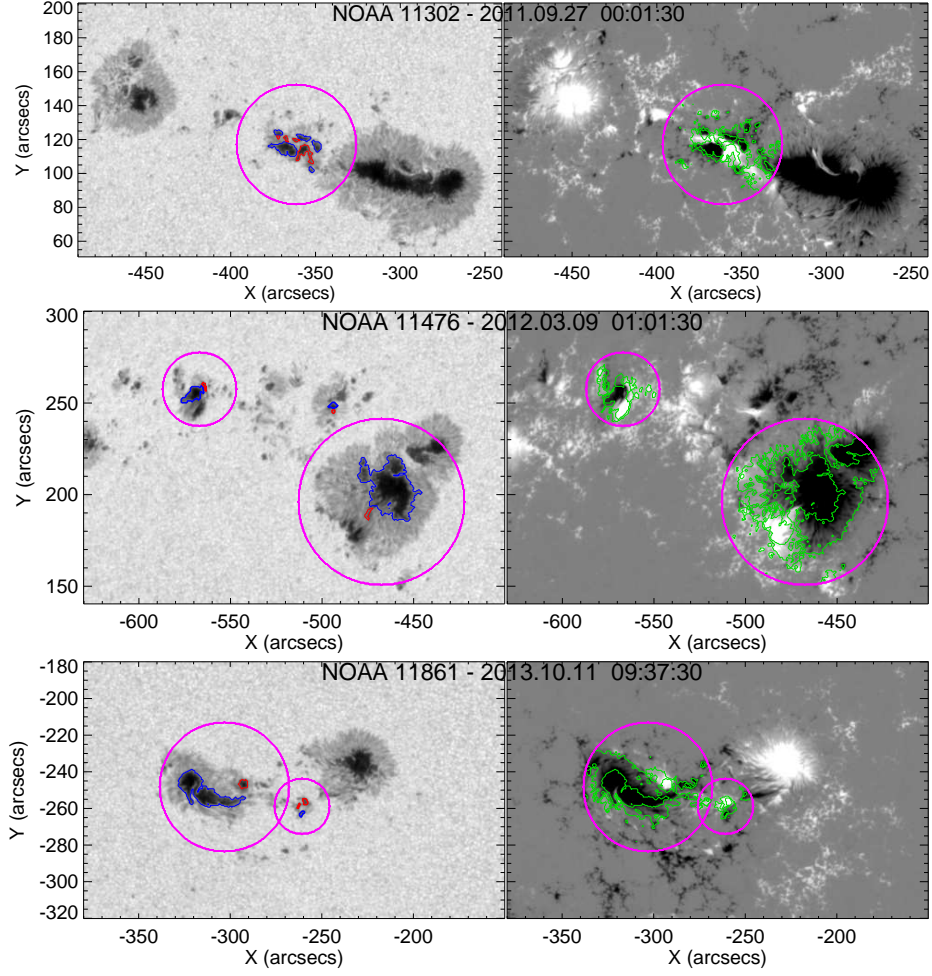


Figure 3. An example of a δ spot detected using the automatic code. The red (blue) contours show the positive (negative) umbrae and the green contours mark the penumbral border. A pink circle surrounds the location of a detected δ configuration.

having positive polarity. The δ formation occurs in the region of flux emergence between the two main spots. It is also observed in this case that the δ spot is formed by multiple small umbrae with opposite polarity and having a rudimentary penumbra around the whole region. A similar configuration is observed in the emerging region, but with two distinct, large and stable bipolar spots in the bottom right image of Figure 1. The central row of the Figure 3 shows another case of two distinct δ spot formations in the same AR. One occurs in the emerging-flux region, similar to the earlier case. Another δ is formed by a small positive-polarity spot joining with a large negative leading-spot. Both spots share a common penumbra surrounding both polarities. The fourth example of a δ spot detected by SMART-DF is given in the bottom row of Figure 3. Two δ forming pairs can be seen here. One of them is similar to the above example,

where a small positive-polarity spot joins with a large, stable negative-polarity spot. In some cases opposite polarities of a small bipolar region may approach each other and form a rudimentary penumbra for a short time. SMART-DF indicates them as a δ since they satisfy both required conditions, and hence are marked with a small circle in the figure (bottom row). Such cases are generally seen at locations of flux emergence. A user can choose to avoid the detection of such small-scale and transient δ spots by increasing the cut-off umbral-area threshold (A_{\min}).

The success rate of δ detection was also tested by comparing with the detections by NOAA/SWPC. There are two methods of performing this comparison, as explained in Section 3. The first method of testing is to check whether each AR is detected by both NOAA and SMART-DF on its first day of observation. During 2011–2012, NOAA’s SRS files reported 33 ARs as having a δ pair at some part of their appearance on the solar-disc. Out of these, 23 ARs formed a δ within $\pm 60^\circ$ longitude. SMART-DF detected 21 out of these 23 NOAA detections several hours before the SRS was released by NOAA. The algorithm failed to detect any δ regions in NOAA AR 11164 and NOAA AR 11374 when compared to SRS. Both were manually checked, on AR 11164 there was not enough penumbra at the beginning when the opposite polarities were within 2° , and by the time the penumbra developed the opposite polarities drifted away to more than the cut-off distance of 2° . In the case of AR 11374 the negative polarity around the positive spot was spread like a plage and did not form a sunspot with area more than A_{\min} .

The second method of testing is to compare the number of instances of daily δ detections by NOAA and SMART-DF. The δ configuration in an AR may remain so for more than one day, and it will be counted again as another instance by both SMART-DF and NOAA. To match with NOAA’s daily SRS, SMART-DF counts each δ region only once *per* day (though SMART-DF uses a cadence of two observation *per* day). During the two years studied here, NOAA detected 97 instances of δ formation within $\pm 60^\circ$ of longitude while the SMART-DF detected 116 cases. Distributions of the two are given in Figure 4. In these additional detections by SMART-DF, five ARs were never reported by NOAA. It is possible that NOAA ground-based data did not show a δ spot, due to its inferior spatial resolution or possible increased seeing. Since only two instances *per* day (at 00:00 UT and 12:00 UT) were used by SMART-DF for analysis, if a δ spot formed and disappeared between the two instances (with a gap of 12 hrs), SMART-DF would have missed that case, while NOAA would have detected them as they scan through out the day. A higher cadence data analysis would show a better match in the distribution. At the same time, SMART-DF may detect small, instantaneous δ s which may be missed, or ignored by manual analysis by NOAA. When multiple δ configurations are formed in the same AR, both SMART-DF and NOAA list count them as one.

5. Discussion and Conclusions

In this article we report on the development of SMART-DF, an algorithm to automatically detect δ spots in active regions. These forms of sunspot groups are

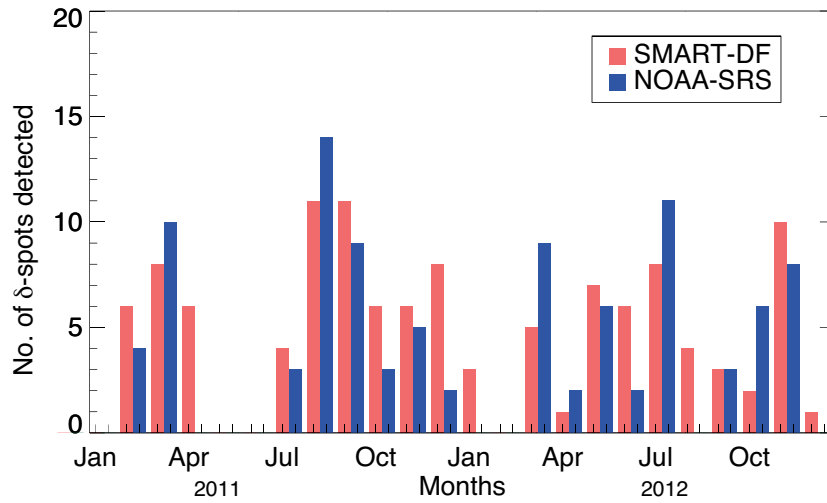


Figure 4. Number of δ spots detected by SMART-DF and NOAA every month of 2011 – 2012. Red bars represent the SMART-DF detection and blue bars represent the detections by NOAA SRS. SMART-DF detected 116 instances of δ spots when compared to 97 by NOAA during 2011 – 2012.

known to be associated with major solar flares (Sammis, Tang, and Zirin, 2000). Current methods to identify δ spots are primarily based on manual checking of ground-based data (*e.g.*, NOAA). Our near-realtime detection of the formation of δ spots can be used to flag an AR as a potential flaring region. SMART-DF will be integrated into SolarMonitor², and hence will be available to the public.

The results of comparing SMART-DF and NOAA/SWPC δ spot detection rates are presented. It is found that during 2011 and 2012, 21 out of 23 ARs detected by NOAA as δ spots (within $\pm 60^\circ$ longitude) were identified by SMART-DF during the 24-hour period before the SRS release by NOAA (which occurs at 00:30 UT every day). In some cases SMART-DF detected δ spots an entire day (during 24 – 48 hours period) before it was marked as a δ by NOAA. In addition SMART-DF detected five ARs which were never reported by NOAA as δ region. If daily instances of δ detections were to be counted, 97 instances were detected by NOAA compared to SMART-DF 116 cases. SMART-DF might have detected more δ spots if the data had been analysed using higher cadence. In this study, data were obtained only once in 12 hrs, any instance of short term δ formation and disappearance during the interval are missed.

SMART-DF determines that a spot is a δ configuration when two conditions are met: i) opposite polarity umbrae within 2° and ii) common penumbra surrounding both polarity umbrae. However, the conventional definition of δ spots is vague. While the Mt. Wilson Observatory uses the specification of within 2° separation, the initial definition by Künzel (1960, 1965) does not mention any value. The recent appearance of the extremely large region NOAA AR 12192 was one specific case where the distance between opposite polarity umbrae (both

²www.solarmonitor.org

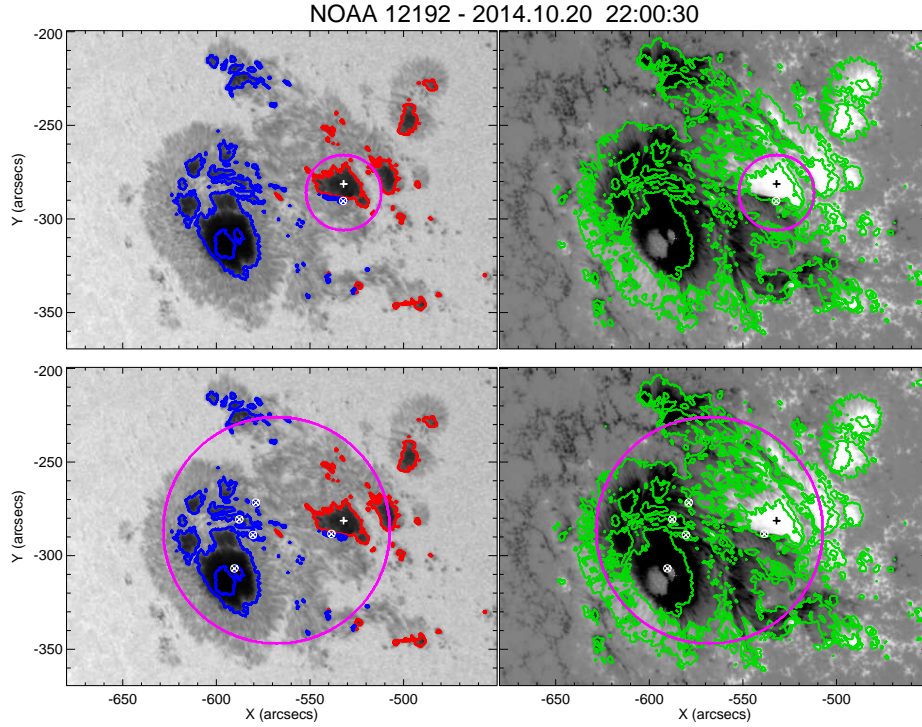


Figure 5. HMI observation of AR12192 and its analysis by SMART-DF. The top and bottom rows of the figure represent two cases with different values for the maximum allowed distance between opposite polarity umbrae (to be detected as a δ spot). The top row is with standard definition value of 2° , and the bottom row is with a value of 5.2° . Red (blue) contours show the positive (negative) umbrae and green contours mark the penumbral border. A circle surrounds the location of a detected δ configuration.

between their centroids and between their closest edges) is more than 2° . As shown in the top row of Figure 5, SMART-DF fails to find the correct δ spot pair (*i.e.*, the two largest umbrae), instead selects a dark and very small negative-polarity region on the edge of the positive-polarity umbra. The correct pair of umbrae was detected only when the restriction of distance was increased, with the bottom row of Figure 5 the result when separations of up to 5.1° are allowed. Although large ARs like AR 12192 are not common, there may be several candidates in which SMART-DF failed because the umbrae separation was slightly more than 2° . In addition, the definition of penumbrae has changed significantly during the last decade with the advent of high-spatial resolution observations. In earlier observations, any shadow-like region around an umbra (with intensity less than the quiet Sun, but more than the umbra) was called penumbra. More recently, penumbrae are known to have distinct filamentary structure with a well defined magnetic topology. SMART-DF, like most other algorithms, uses only intensity values around umbrae to identify penumbrae. When two pores are in close proximity, a shadow-like region can form between them with an intensity between that of the quiet Sun and the pores (*i.e.*, umbrae). Currently, SMART-

DF will identify this as a penumbra and may use that to satisfy the second δ spot condition.

The detection of a δ spot does not assure the occurrence of a flare, but for flare forecasting studies it will be important to determine how useful δ spot detection is in identifying potentially flaring ARs. In a follow-on study, SMART-DF will be used to investigate the evolution of different physical parameters in δ spots, including the observed changes in magnetic topology and plasma velocity.

Acknowledgments This work has received financial support from: EOARD (SP), Irish Research Council- Enterprise partnership (PAH), European Space Agency Prodex programme (DSB). Courtesy of NASA/SDO and the HMI science teams for the data used in this paper.

References

- Ahmed, O.W., Qahwaji, R., Colak, T., Higgins, P.A., Gallagher, P.T., Bloomfield, D.S.: 2013, Solar Flare Prediction Using Advanced Feature Extraction, Machine Learning, and Feature Selection. *Solar Phys.* **283**, 157. DOI. ADS.
- Allen, C.W.: 1976, *Astrophysical Quantities*. Athlone Press. London. ADS.
- Aschwanden, M.J., Freeland, S.L.: 2012, Automated Solar Flare Statistics in Soft X-Rays over 37 Years of GOES Observations: The Invariance of Self-organized Criticality during Three Solar Cycles. *Astrophys. J.* **754**, 112. DOI. ADS.
- Barnes, G., Leka, K.D.: 2008, Evaluating the Performance of Solar Flare Forecasting Methods. *Astrophys. J. Lett.* **688**, L107. DOI. ADS.
- Barra, V., Delouille, V., Kretzschmar, M., Hochedez, J.-F.: 2009, Fast and robust segmentation of solar EUV images: algorithm and results for solar cycle 23. *Astron. Astrophys.* **505**, 361. DOI. ADS.
- Bloomfield, D.S., Higgins, P.A., McAteer, R.T.J., Gallagher, P.T.: 2012, Toward Reliable Benchmarking of Solar Flare Forecasting Methods. *Astrophys. J. Lett.* **747**, L41. DOI. ADS.
- Colak, T., Qahwaji, R.: 2008, Automated McIntosh-Based Classification of Sunspot Groups Using MDI Images. *Solar Phys.* **248**, 277. DOI. ADS.
- Colak, T., Qahwaji, R.: 2009, Automated Solar Activity Prediction: A hybrid computer platform using machine learning and solar imaging for automated prediction of solar flares. *Space Weather* **7**, 6001. DOI. ADS.
- Conlon, P.A., Gallagher, P.T., McAteer, R.T.J., Ireland, J., Young, C.A., Kestener, P., Hewett, R.J., Maguire, K.: 2008, Multifractal Properties of Evolving Active Regions. *Solar Phys.* **248**, 297. DOI. ADS.
- Cui, Y., Li, R., Zhang, L., He, Y., Wang, H.: 2006, Correlation Between Solar Flare Productivity and Photospheric Magnetic Field Properties. 1. Maximum Horizontal Gradient, Length of Neutral Line, Number of Singular Points. *Solar Phys.* **237**, 45. DOI. ADS.
- Curto, J.J., Blanca, M., Martínez, E.: 2008, Automatic sunspots detection on full-disk solar images using mathematical morphology. *Solar Phys.* **250**(2), 411. DOI. ADS.
- Emslie, A.G., Dennis, B.R., Shih, A.Y., Chamberlin, P.C., Mewaldt, R.A., Moore, C.S., Share, G.H., Vourlidas, A., Welsch, B.T.: 2012, Global Energetics of Thirty-eight Large Solar Eruptive Events. *Astrophys. J.* **759**, 71. DOI. ADS.
- Freeland, S.L., Handy, B.N.: 1998, Data Analysis with the SolarSoft System. *Solar Phys.* **182**, 497. DOI. ADS.
- Gallagher, P.T., Moon, Y.-J., Wang, H.: 2002, Active-Region Monitoring and Flare Forecasting I. Data Processing and First Results. *Solar Phys.* **209**, 171. DOI. ADS.
- Gopalswamy, N., Barbieri, L., Lu, G., Plunkett, S.P., Skoug, R.M.: 2005, Introduction to the special section: Violent Sun-Earth connection events of October-November 2003. *Geophys. Res. Lett.* **32**, 3. DOI. ADS.
- Greisen, E.W., Calabretta, M.R.: 2002, Representations of world coordinates in FITS. *Astron. Astrophys.* **395**, 1061. DOI. ADS.
- Hale, G.E., Ellerman, F., Nicholson, S.B., Joy, A.H.: 1919, The Magnetic Polarity of Sun-Spots. *Astrophys. J.* **49**, 153. DOI. ADS.

- Hapgood, M., Thomson, A.: 2010, *Space weather: Its impact on earth and implications for business*, Lloyd's 360 Risk Insight, London.
- Higgins, P.A., Gallagher, P.T., McAteer, R.T.J., Bloomfield, D.S.: 2011, Solar magnetic feature detection and tracking for space weather monitoring. *Adv. in Space Res.* **47**, 2105. DOI. ADS.
- Künzel, H.: 1960, Die Flare-Häufigkeit in Fleckengruppen unterschiedlicher Klasse und magnetischer Struktur. *Astron. Nach.* **285**, 271. ADS.
- Künzel, H.: 1965, Zur Klassifikation von Sonnenfleckengruppen. *Astron. Nach.* **288**, 177. ADS.
- LaBonte, B.J., Georgoulis, M.K., Rust, D.M.: 2007, Survey of Magnetic Helicity Injection in Regions Producing X-Class Flares. *Astrophys. J.* **671**, 955. DOI. ADS.
- Lefebvre, S., Rozelot, J.-P.: 2004, A new method to detect active features at the solar limb. *Solar Phys.* **219**, 25. DOI. ADS.
- Leka, K.D., Barnes, G.: 2007, Photospheric Magnetic Field Properties of Flaring versus Flare-quiet Active Regions. IV. A Statistically Significant Sample. *Astrophys. J.* **656**, 1173. DOI. ADS.
- Leka, K.D., Skumanich, A.: 1998, The Evolution of Pores and the Development of Penumbrae. *Astrophys. J.* **507**, 454. DOI. ADS.
- Martens, P.C.H., Attrill, G.D.R., Davey, A.R., Engell, A., Farid, S., Grigis, P.C., Kasper, J., Korreck, K., Saar, S.H., Savcheva, A., Su, Y., Testa, P., Wills-Davey, M., Bernasconi, P.N., Raouafi, N.-E., Delouille, V.A., Hochedez, J.F., Cirtain, J.W., Deforest, C.E., Angryk, R.A., de Moortel, I., Wiegmann, T., Georgoulis, M.K., McAteer, R.T.J., Timmons, R.P.: 2012, Computer Vision for the Solar Dynamics Observatory (SDO). *Solar Phys.* **275**, 79. DOI. ADS.
- McAteer, R.T.J., Gallagher, P.T., Ireland, J., Young, C.A.: 2005, Automated Boundary-extraction And Region-growing Techniques Applied To Solar Magnetograms. *Solar Phys.* **228**, 55. DOI. ADS.
- McIntosh, P.S.: 1990, The classification of sunspot groups. *Solar Phys.* **125**, 251. DOI. ADS.
- Messerotti, M., Zuccarello, F., Guglielmino, S.L., Bothmer, V., Lilensten, J., Noci, G., Storini, M., Lundstedt, H.: 2009, Solar Weather Event Modelling and Prediction. *Space Sci. Rev.* **147**, 121. DOI. ADS.
- Moore, R.L., Sterling, A.C., Hudson, H.S., Lemen, J.R.: 2001, Onset of the Magnetic Explosion in Solar Flares and Coronal Mass Ejections. *Astrophys. J.* **552**, 833. DOI. ADS.
- Nordlund, Å., Stein, R.F., Asplund, M.: 2009, Solar Surface Convection. *Living Reviews in Solar Phys.* **6**, 2. ADS.
- Sammis, I., Tang, F., Zirin, H.: 2000, The Dependence of Large Flare Occurrence on the Magnetic Structure of Sunspots. *Astrophys. J.* **540**, 583. DOI. ADS.
- Scherrer, P.H., Schou, J., Bush, R.I., Kosovichev, A.G., Bogart, R.S., Hoeksema, J.T., Liu, Y., Duvall, T.L., Zhao, J., Title, A.M., Schrijver, C.J., Tarbell, T.D., Tomczyk, S.: 2012, The Helioseismic and Magnetic Imager (HMI) Investigation for the Solar Dynamics Observatory (SDO). *Solar Phys.* **275**, 207. DOI. ADS.
- Smart, W.M.: 1965, *Text-book on spherical astronomy*. Cambridge univ. press. ADS.
- Solanki, S.K.: 2003, Sunspots: An overview. *Astron. Astrophys. Rev.* **11**, 153. DOI. ADS.
- Thompson, W.T.: 2006, Coordinate systems for solar image data. *Astron. Astrophys.* **449**, 791. DOI. ADS.
- Verbeeck, C., Higgins, P.A., Colak, T., Watson, F.T., Delouille, V., Mampaey, B., Qahwaji, R.: 2013, A Multi-wavelength Analysis of Active Regions and Sunspots by Comparison of Automatic Detection Algorithms. *Solar Phys.* **283**, 67. DOI. ADS.
- Watson, F., Fletcher, L., Dalla, S., Marshall, S.: 2009, Modelling the Longitudinal Asymmetry in Sunspot Emergence: The Role of the Wilson Depression. *Solar Phys.* **260**, 5. DOI. ADS.
- Yuan, Y., Shih, F.Y., Jing, J., Wang, H.-M.: 2010, Automated flare forecasting using a statistical learning technique. *Research in Astronomy and Astrophysics* **10**, 785. DOI. ADS.
- Zharkov, S., Zharkova, V., Ipson, S., Benkhalil, A.: 2004, Automated recognition of sunspots on the soho/mdi white light solar images. In: Negoita, M., Howlett, R., Jain, L. (eds.) *Knowledge-Based Intelligent Information and Engineering Systems, Lect. Notes in Comp. Sci.* **3215**, Springer Berlin Heidelberg, ISBN 978-3-540-23205-6. DOI.